PLOS WATER

RESEARCH ARTICLE

A framework for modelling emergent sediment loss in the Ombrone River Basin, central Italy

Nazzareno Diodato[1], Fredrik Charpentier Ljungqvist[2,3,4]*, Francesco Fiorillo[5], Gianni Bellocchi[6]

1 Met European Research Observatory–International Affiliates Program of the University Corporation for Atmospheric Research, Benevento, Italy, **2** Department of History, Stockholm University, Stockholm, Sweden, **3** Bolin Centre for Climate Research, Stockholm University, Stockholm, Sweden, **4** Swedish Collegium for Advanced Study, Linneanum, Uppsala, Sweden, **5** Department of Science and Technologies, University of Sannio, Benevento, Italy, **6** VetAgro Sup, INRAE, Université Clermont Auvergne, Clermont-Ferrand, France

* fredrik.c.l@historia.su.se

Citation: Diodato N, Ljungqvist FC, Fiorillo F, Bellocchi G (2023) A framework for modelling emergent sediment loss in the Ombrone River Basin, central Italy. PLOS Water 2(2): e0000072. https://doi.org/10.1371/journal.pwat.0000072

Editor: Sher Muhammad, ICIMOD: International Centre for Integrated Mountain Development, NEPAL

Received: September 24, 2022

Accepted: January 2, 2023

Published: February 1, 2023

Data Availability Statement: Uploaded as supplementary information.

Funding: FCL was supported by the Swedish Research Council (Vetenskapsrådet, grant no. 2018-01272) and conducted the work with this article as a Pro Futura Scientia XIII Fellow funded by the Swedish Collegium for Advanced Study through Riksbankens Jubileumsfond. The funders had no role in study design, data collection and analysis, decision to publish, or preparation of the manuscript.

Abstract

Water can represent a hazard causing soil erosion and it is essential to anticipate the potential environmental impacts of sustained rainwater energy to achieve sustainability. Here, we present the modelling of the erosive force of water for the production of soil sediment in a Mediterranean basin of central Italy (Ombrone River Basin, ORB). A point of departure is the historical recognition of the environmental factors causing sediments loss (SL) by water. A semi-empirical framework was then proposed for the upscaling of SL based on the Foster-Thornes approach (EUSEM: Environmental Upscaling Sediment Erosion Model) in order to give an insight into annual sediment losses (SL) over the period 1949–1977 (calibration) and over a longer time-frame (1942–2020: reconstruction). Two change-points were detected: 1967 and 1986. During this period, SL was affected by a sharp decrease from 625 Mg km^{-2} yr^{-1}, before the first change-point (when SL was only occasionally below the tolerable soil loss threshold of 150 Mg km^{-2} yr^{-1}), to 233 Mg km^{-2} yr^{-1}, during the transition phase 1967–1985 (mostly above the warning treshold of 140 Mg km^{-2} yr^{-1}). This decrease coincided with an enhancing of vegetation throughout the basin due to an ongoing afforestation process. After this period, a resurgence of climatic forcing led to a further, but more contained, increase in SL, from 1996 onwards. This case-study illustrates the application and results that can be obtained with the framework for the outcome of environmental change due to sediment losses in a Mediterranean fluvial basin. Limitations and perspectives of this approach are given as conclusion.

1. Introduction

Despite considerable advances in model-based work on the resposse of sediment erosion to climatic and other environmental changes, research is still confronted with the need to produce

Competing interests: The authors have declared that no competing of interest exist.

experimental evidence on the erosional dynamics associated with long-term responses [1]. The strength and temporal progression of erosion-sediment can have a major impact on landscape layout through long-term environmental pressures [2], as erosion of agricultural land in many regions is rapidly degrading soil at a faster rate than its natural renewal [3]. Studies show that soil erosion by running water depends mainly on rainfall intensity and duration, soil properties, vegetation, land use and antecedent soil wetting conditions [4, 5]. Although the effects of wind on soil erosion can be severe in arid and semi-arid areas [6], wind erosion is less than water erosion on a global scale [7]. Water represents perhaps the most challenging aspect compared to the other elements [8], due to its unpredictability [9], the power of rainfall and its aggressiveness related to runoff and flooding [10].

Hydrological extremes have widespread, often harmful, impacts on ecosystems resulting in soil losses and economic damage [11], especially in the Mediterranean region [12]. The Mediterranean region, in fact, experienced signifcant climatic variations during the Holocene period (last ~11,700 years). The Little Ice Age (LIA, ~1250–1850 CE) featured in the Mediterranean region prolonged wet intervals [13], which had important consequences for terrestrial ecosystems [14]. In fact, during 16th century the process of extension of ploughing on the hilly soils, which had already started in the 12th century, developed further, involving new areas further away from inhabited centers, and expanding more and more often also to uplands [15, 16]. Fig 1A gives us an image of the erosion of the shallow slopes and, at the same time, of the deforested areas upstream of the Ombrone River Basin (ORB), which is the focus of this study.

The timing and extent of the transition from the mid-19th centrury and the onset of the current warmer and, in the study region, drier climatic conditions have led to a stabilisation of the landscape, to which human reforestation has contributed (Fig 1B and 1C). However, erosional soil degradation remains a subject of much debate due to the timing and erraticity of extreme hydrological events accompanying this phase of climate change. For instance, erosion studies have focused on long-term mean areal estimates [17–19], on short time-series [20, 21], or even on scattered years [22], leaving unexamined the historical evolution of erosional sediment transport in the landscapes of many Tuscan river basins.

Fig 2 illustrates the spatial pattern of soil erosion in 2012. Over the 21st century, the global mean amount of potential soil erosion has increased (+2.5% from 35.0 Pg yr^{-1} in 2001 to

Fig 1. Historical evolution of the landscapes in the Ombrone River Basin. a) The degradation of the hilly and mountainous landscape of Gavinana (43˚ 56' N, 10˚ 55' E) during the 16th century in the painting *Presa di Gavinana* (1556–1562), a fresco from the school of Giorgio Vasari (1511–1574), available free of charge from the *Fondazione Federico Zeri*, *Università di Bologna* (http://catalogo.fondazionezeri.unibo.it/scheda/opera/39379/Stradano%20Giovanni%2C%20Battaglia%20tra%20le%20truppe%20fiorentine%20e%20imperiali), b) wooded landscape with Mount Amiata reforestation area (photo of the *Archivio Italia Nostra*, from *I paesaggi rurali storici della Toscana*, from Regione Toscana, 2014b, p. 9 [89], freely available at https://www.regione.toscana.it/-/piano-di-indirizzo-territoriale-con-valenza-di-piano-paesaggistico), c) stable agricultural and forest landscape of high naturalistic value in the upper valley if Albegna River, near Murci (42˚ 44' N, 11˚ 24′ E), in the province of Grosseto (photo taken by A. Chiti-Batelli, archive NEMO, from Regione Toscana, 2014b, p. 29 [89], freely available at https://www.regione.toscana.it/-/piano-di-indirizzo-territoriale-con-valenza-di-piano-paesaggistico).

https://doi.org/10.1371/journal.pwat.0000072.g001

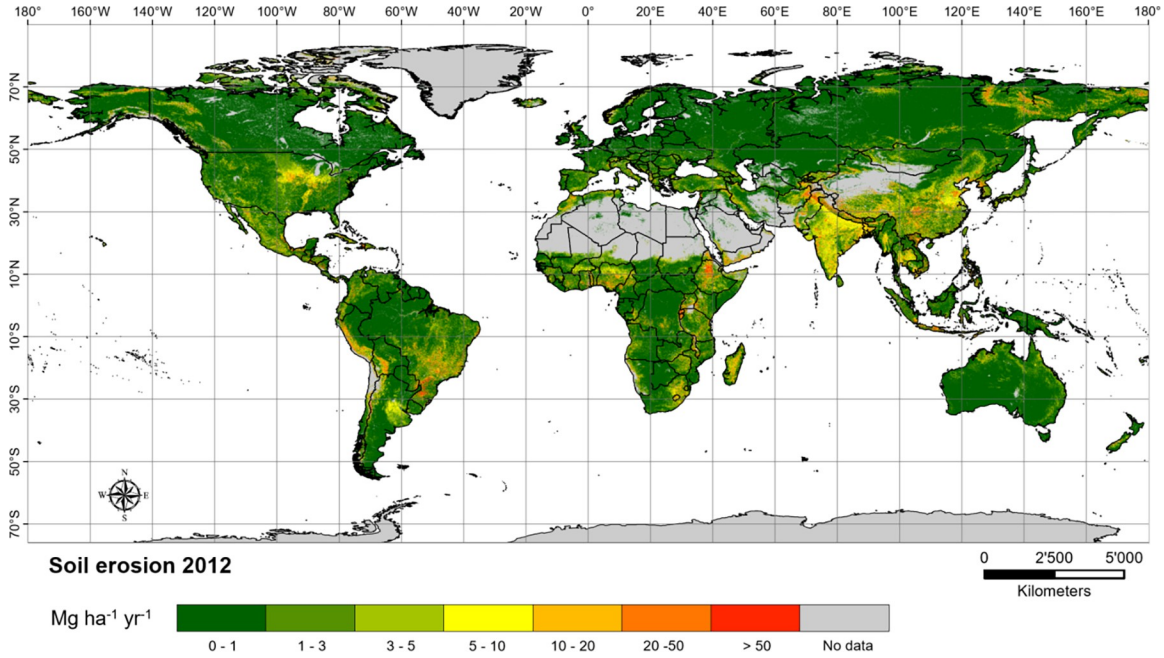

Fig 2. Global soil erosion in 2012, based on estimates through a (R)USLE-based modelling approach integrated in a geographic information system environment [23]. Image freely available from Global Soil Erosion Modelling platform (GloSEM)-European Soil Data Centre (https://esdac.jrc.ec.europa.eu/themes/global-soil-erosion; Borrelli et al. [23, 90]).

https://doi.org/10.1371/journal.pwat.0000072.g002

35.9 Pg yr^{-1} 2012), mainly driven by land-use changes, such as the decline of forests and the expansion of semi-natural vegetation and cropland [23]. In addition, hydrological systems in different river basins worldwide have come under increasing pressure on land resources due to urbanisation and poor land management practices [24], as well as changes in precipitation patterns [25].

Tuscany has become one of the most vulnerable regions in Italy [26], with most of its territory classified as being at high risk of erosion [27]. In fact, in recent decades, extreme weather-climatic events have highlighted the effects of ongoing climate change indicating a trend towards an increase in very intense precipitation events that may have important repercussions on the territory from a hydrogeological point of view [28]. For instance, the ORB has been affected by extreme events in the past decade, such as during the Grosseto provinceflood of November 12, 2012, which altered the soil properties that regulate plant and animal life, causing heavy economic losses [29]. Intense rainfall also affected the Mount Amiata area, including the Senese slope, with daily pluviometric values advancing between *c*. 100 and 400 mm in the 2010–2020 period from the north (near Siena) to the south (near the coast) of the Ombrone basin [30]. Between October 18 and 21, 2014, another major flood was recorded, leading to the closure of the Grosseto-Siena railway line [31]. However, already in the past, many ORB lands were affected by remarkable erosive processes, especially under the pressure of deforestation of the Apennines, as reconstructed by historians of the time (ARAAT, 1904, p. 268 [32], our translation):

The deforestation that is often carried out indiscriminately in the Apennines [. . .], while very harmful in various respects, has instead increased the richness of the solid material [. . .]. I remember, for example, the Ombrone which, after increased deforestation, saw the amount of sediment increased [by 23%].

Today, the use of satellite remote sensing for soil erosion mapping and modelling has received considerable attention [33], but these records tend to cover single events up to, at

most, a few decades [34]. Thus, the short periods of these records mean that we cannot assess whether the spatial patterns associated with erosion initiation events persist over the time-scales that are notable for landscape change and evolution [35]. To operate over extended time periods, models engaged in soil erosion require, however, a variety of environmental inputs as well as comprehensive parameterisation. In this context, the application of dynamic and physical models is often illusory due to a lack of detailed data required for these types of models when going back in time. A challenge is to find out how climate variability affects soil erosion over interdecadal and longer time scales. In fact, sediment discharge data on such long time scales are scarcely available for most river basins [36] and this motivates the development of hydrological models to reconstruct the long-term variability of sediment data at the scale of basins with relatively low data availability. Semi-empirical models developed to assess sediment loss at the basin scale use environmental factors to characterise drainage basins in terms of sensitivity to rainfall erosivity and sediment transport [37]. They consider erosion processes to some extent with a limited amount of data, which makes them suitable for estimating in-basin effects on soil erosion [38]. In particular, parsimonious mathematical models can simulate the combined effects of hydroclimatic forcing agents, such as the estimation of sediment budgets using–in the absence of spatially and temporally distributed data–the drainage basin as a homogeneous landscape unit in which sediment fluxes and land surface changes can be calculated [39].

The classical soil erosion determination procedure of Wischmeier and Smith [40], the Universal Soil Loss Equation and its revised forms–(R)USLE [41]–or its WaTEM/SEDEM extension to continental scale [42] are applicable to the calculation of long-term mean annual erosion, but their use at basin level for estimating annual soil loss values from single storms has led to a reinterpretation of the original formulation [43]. This has allowed the identification of concepts for the development of parsimonious modelling solutions for sediment load assessment of river systems [44–47]. Given the issue of assessing erosive sediment by complex models in recognition of the detailed input for the historical period, we arranged a parsimonious erosion model adapted to the annual scale from the original algorithms of Foster et al. [48] and Thornes [49] because they provide an interpretation of empirically determined factors shaping active erosional landscapes in basin areas based on the parsimonious balance between driving and resisting forces in the sediment budget [50, 51]. The driving forces are essentially simplified to proxies or indicators or rainfall and runoff erosivity associated with splash and transport erosion, respectively. This simplification seems to be adequate for the generation of basin-wide annual outputs, while it may not be fully applicable for the generation of monthly outputs, as seasonal effects become prominent due to the concurrence of rainfall erosivity with different seasonal conditions of soil erodibility [50, 51]. Resisting forces are expressed as an exponential function of the fraction of vegetation cover in the basin, as erosion rates show a steep decay compared to that of a bare soil as plant cover increases [52]. This relatively simple approach is desirable to reconstruct interannual and interdecadal variability in the evolution of landscape responses over periods of several decades in historical time, for which only monthly and daily rainfall amounts can be used. Empirical models to be applied–even if based on simple physical concepts–are much more attractive from an interdisciplinary point of view as they are able to capture the attention of a wide range of environmental scientists, where engineers, physicists, agronomists, historians, geographers, ecologists and geomorphologists can interact more easily than physically-based models. This is also so due to the interaction between variables which, in empirical models, are more explicit, in contrast to physical models where often the interaction mechanisms are locked in complex algorithms that are difficult to understand for a group of people with different and not-specialised knowledge. In this way,

simple models can also integrate the work of several research groups into a single working product that summarises understanding [53].

Our objective was to reconstruct the dynamics of sediment loss in the ORB from a parsimonious interpretation of the relationship between input data and a basin-responsive erosion variable. The adoption of a parsimonious model is motivated by its ability to capture important environmental changes (including temperature, land cover and erosive resistance properties) using readily available data. The ability to reproduce (at basin scale) the combined effects of hydro-climatological processes, including sediment transport, in the absence of distributed spatial and temporal data, relies on the possibility of considering a drainage basin as a homogeneous ecosystem unit, counting only on two stations with continuous and homogeneous data. The sediment loss time-series, with a total of 28 sediment samples from Sasso d'Ombrone station (derived from the former SIMN dataset [54]), offered a unique opportunity to explore erosion processes in the basin. Thus, for the first time, it was possible to apply this approach to reconstruct the sediment loss from the Ombrone River Basin (ORB), over the 1942–2020 period.

2. Materials and methods

2.1. Environmental setting, data and methods

The Ombrone River Basin (ORB) is located in the part of central Italy facing the Tyrrhenian Sea (Fig 3A, black rectangle). With a length of 161 km, the Ombrone is the second main river of Tuscany after the Arno (241 km). It crosses its southernmost part from north to south, up to its middle valley, and then turns south-west, until it reaches its delta, in the municipality of Grosseto (42˚ 46' N, 11˚ 06˚ E). The Ombrone River has the highest flow of suspended solid

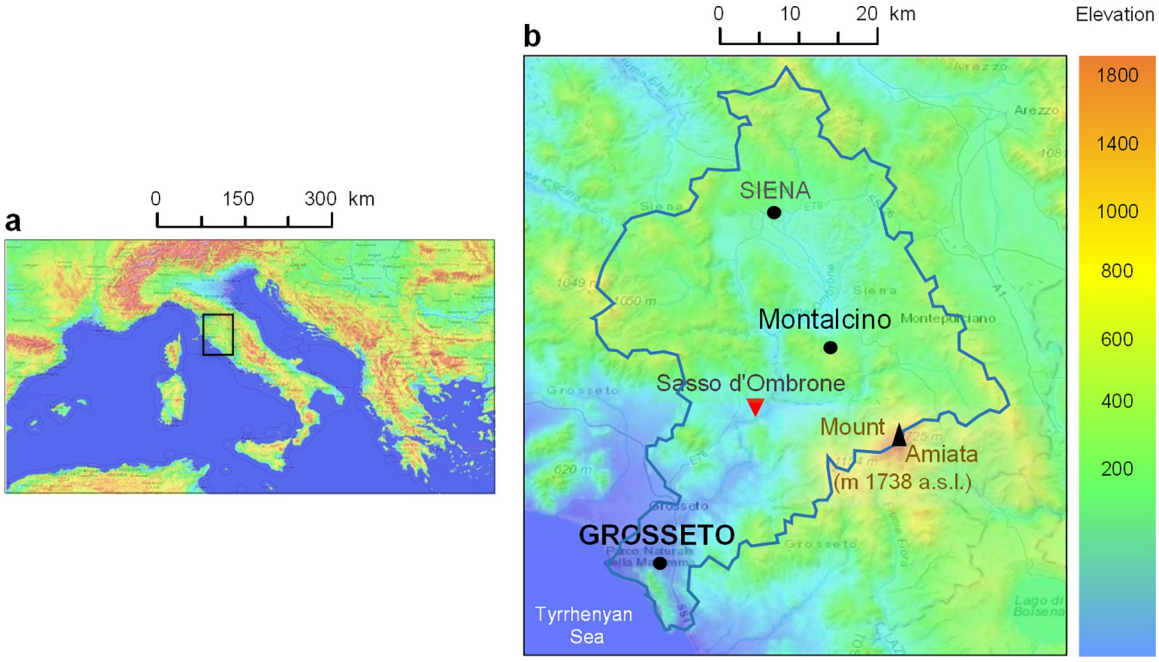

Fig 3. The Ombrone River Basin. a) Geographical setting (black rectangle) within the central Mediterranean region, with b) the basin boundaries (bold blue line) with the main river network. The climatic reference stations of Grosseto (42˚ 46' N, 11˚ 06˚ E) and Montalcino (43˚ 03′ N, 11˚ 29′ E), the main city of Siena (43˚19′ N, 11˚19′ E) (black dots), the sediment measurement station of Sasso d'Ombrone (red triangle) and the highest peak of Mount Amiata (42˚ 54′ N, 11˚ 38′ E), are highlighted. Both maps are output images created from topographic-map (https://it-it.topographic-map.com/maps/klqe/Europa).

https://doi.org/10.1371/journal.pwat.0000072.g003

sediment among the Tuscan rivers. This is due to the high erodibility of the rocks on which the river establishes its course. The surface area of its basin is 3494 km^2, but the area over which sediment production is collected is 2656 km^2 (Sasso d'Ombrone, Fig 3B). It receives several tributaries, including, on the hydraulic right, the Arbia, which rises on the slopes of the Caballari hill (648 m a.s.l.), near Castellina in Chianti, in the province of Siena, and flows into the Ombrone at Buonconvento, the Merse, 70 km long, which originates on the Croce di Prata hill and flows into the Ombrone shortly after receiving the Farma (its first tributary) at Piani di Rocca, the Gretano and the Lanzo. The left-hand tributaries of the Ombrone are the Melacce, the Trasubbie, the Maiano, the Grillese, the Rispescia and the Orcia, which is the most important river with a total basin area of 748 km^2.

In terms of physiography, the ORB has vast areas of hills and mountains with slopes of over 20%, characterised by torrential streams running through narrow valleys of great geomorphological and floristic interest. The decidedly hilly areas are mainly located in the north and east, while in the west there is a rather mountainous, somewhat rugged and structurally complex morphology [28]. The southern edge of the ORB is formed by a morpho-structural ridge which, in a southwest to northeast direction, connects the Uccellina Mountains to Mount Amiata. The elevations of the reliefs are always higher, following the dorsal axis from southwest to northeast, and reach their maximum values in the extreme northeast, corresponding to Mount Labbro (1193 m a.s.l.), the volcanic cone of Mount Amiata (1738 m a.s.l.) and Mount Civitella (1107 m a.s.l.). The middle Ombrone valley winds through slightly elevated and rounded hills, where the initial slope gradient is attenuated, and near Camigliano the course of the river winds through the plain of the countryside (Fig 4).

After the confluence with the Arbia, and after passing through a rocky gorge, the river enters the Grosseto plain which extends on its right, while on the left the riverbed continues to

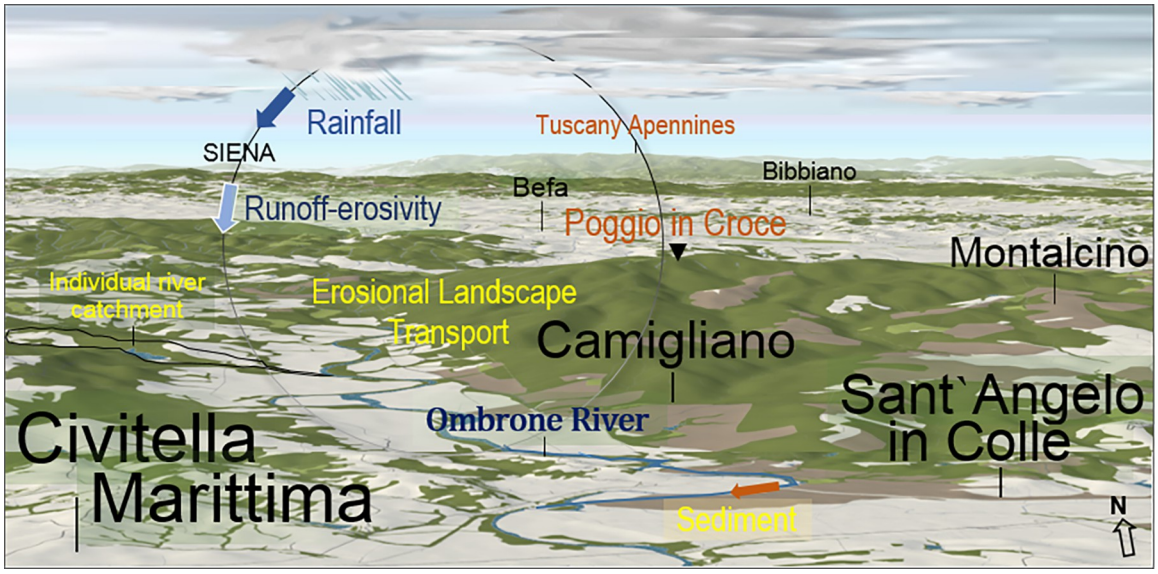

Fig 4. Perspective view of the middle valley of the Ombrone River Basin with the sediment erosion sequence. The meandering Ombrone River (in blue), which rises in the north and disappears on the horizon in the province of Siena, where it rises on the south-eastern slopes of the Chianti Mountains. In its valley there are numerous patches of wooded vegetation (green areas), especially around the hilly terrain, Montalcino being the hydro-climatological reference station of the basin. The process of sediment erosion follows the sequence of rainfall-runoff and erosivity-soil erosion until the loss of sediment. The map is an output image created by the authors from OpenStreetMap (https://demo.f4map.com/#camera.thea=0.9) in which localities are in black, reliefs in ochre, fluvial and hydrogeological processes in blue, and landscape-related processes in yellow.

https://doi.org/10.1371/journal.pwat.0000072.g004

run along the foot of the hills for a while. The landscape depicted in Fig 4 is representative of the territory of the basin, which contains greatly diversified landforms, even if the relationships that mutually link these aspects have given rise to landscape structures of a remarkable internal coherence, which has made them recognisable over time. In terms of land use, the basin is largely affected by wooded areas (~45%), composed mainly of low formations of, broadleaf trees and Mediterranean scrub ("Mediterranean forests, woodlands, and scrub" biome [55]), dominated by tall trees (until at least the first half of the 19th century), forests and semi-natural pastures for raising livestock of various types.

The cultivated areas are mostly open farmland in medium-large enclosed fields, cut into the forest space, often with acorn oaks and bordered by dense trees or tree patches, while a gradual spread–but always as secondary crops depending on farmers' livelihood–of vines and olives in mixed form or in small specialised plants, mostly in the vicinity of inhabited centres and farm-houses, with the presence of chestnut on the highest hills [56].

2.2. Climate and seasonal hydrology

The climatic unit of the ORB is influenced by the Tyrrhenian Sea and its mitigating action, by the overall exposure to the west, and by the protection to the east offered by the Apennine barrier, which contrasts with the infrequent but cold winter currents from the east and northeast. The predominant currents are those from the west and especially those from the northwest, and the wind regime is influenced by the succession of depressions of Mediterranean origin and by the orographic ones during the winter semester: the latter, from October to April, recall the humid currents from the south over Tuscany [57]. These precipitation events are the cause of significant erosive rainfall, which in the ORB ranges around 1500 MJ mm h^{-1} hm^{-2} yr^{-1} in the eastern terrain, and between 1800 and 2000 MJ mm h^{-1} hm^{-2} yr^{-1} in the wider western area (period 2001–2011; Fig 5A).

Erosive rains, together with other predisposing landscape factors, trigger marked soil losses over much of the territory and, in particular, in the eastern parts of the basin (Fig 5B). The monthly climatic regime of two stations taken as reference in the model input data, extending over a longer period, from 1971 to 2010, is characterised by similar trends, with the only exception that the Montalcino station is more continental, with a bimodal-like fluctuation of rainfall, slightly more abundant and with a shorter summer dry period compared to the Grosseto station (Fig 5C and 5D).

Intense summer and autumn precipitation can cause flash-floods in various parts of the basin. These phenomena have a significant impact on the network of hills and mountains, which is characterised by considerable volumes of flood water, as well as significant velocities of propagation and large flooding surfaces. In fact, periods with abundant rainfall generate flood outflows with rates of thousand m^3 s^{-1} (as occurred with peak flows of 3120 m^3 s^{-1} on 02/11/1944 and 3110 m^3 s^{-1} on 04/11/1966, detected at the Sasso d'Ombrone hydrometric station), accompanied by intense erosions of the slopes, alternating with periods of extreme drought, with flows of less than 5 m^3 s^{-1} (as was the case of the minimum flow of 1.10 m^3 s^{-1} in August 1973). The high variability of the regime between these two extreme conditions has made the area more vulnerable, increasing its hydrological risk.

2.3. Data collection

Continuous sediment loss measurements made between 1949 and 1977 at the Sasso d'Ombrone turbidometric station (Fig 3B, red triangle) are a valuable source of information for sediment erosion modelling. In particular, for the pluviometric data, we refer to the data provided by the Tuscany Functional Centre (https://www.cfr.toscana.it). The percentage

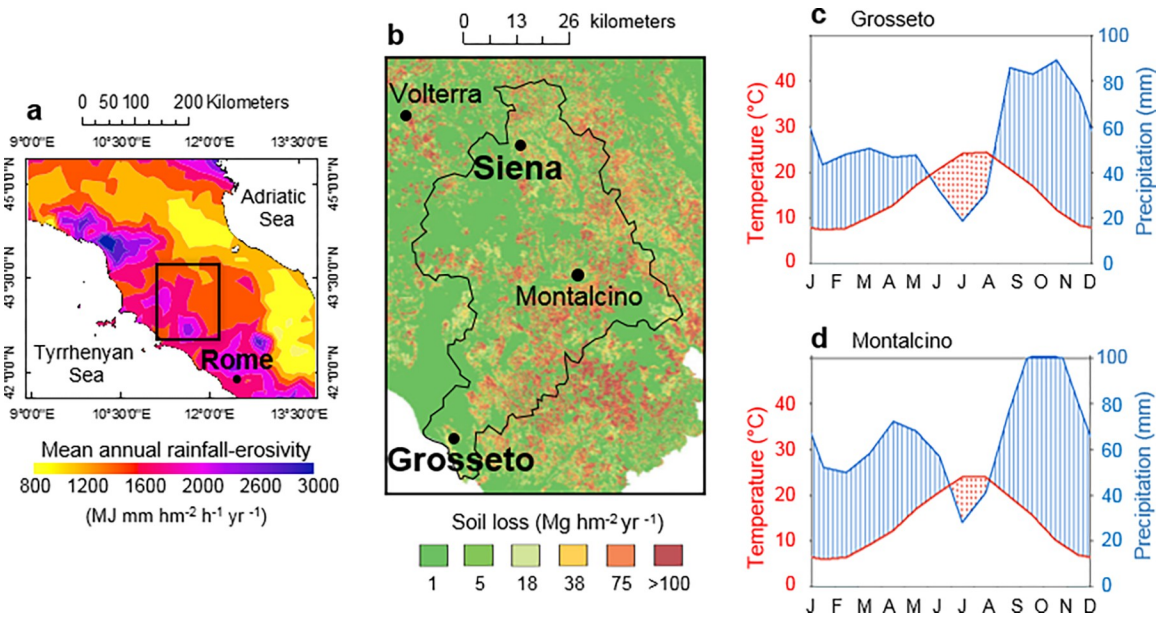

Fig 5. Hydrogeomorphology of the Ombrone River Basin. a) Spatial pattern of mean annual rainfall erosivity in central Italy over the period 2001–2011 (arranged using the ArcGIS cokriging interpolation of ESRI Geostatistical Analyst on the ESDAC-European Soil Data Centre dataset, https://esdac.jrc.ec.europa.eu/content/global-rainfall-erosivity; Panagos et al. [91]), b) long-term soil erosion rate (modified from Angeli et al. [92]), c) Walther-Lieth diagram for the Grosseto station, and d) for the Montalcino station (arranged from LaMMA-*Laboratorio di Monitoraggio e Modellistica Ambientale per lo sviluppo sostenibile*, http://www.lamma.rete.toscana.it/clima-e-energia/climatologia). The units adopted for rainfall erosivity (MJ mm hm^{-2} h^{-1} yr^{-1}) and soil loss (Mg hm^{-2} yr^{-1}) refer to a land area of 10,000 m^{-2} (1 hm^{-2}), the hectare (1 ha, equal to 1 hm^{-2}) not being a metric unit in the international system.

https://doi.org/10.1371/journal.pwat.0000072.g005

vegetation cover was, in both the calibration and reconstruction stages, extracted from the HYDE 3.2 dataset [58].

2.4. Model development

Following Mulligan and Wainvright [53], our model building has involved compartmentalising the issue and specifying it as compartments and flows for an initial test towards a satisfactory solution. Sediment loss, also known as net erosion, is the amount of sediment from all sources of soil erosion, minus sediment trapped on floodplains, that passes through the outlet of a river basin [59]. The sum is the sediment displaced downstream to the basin outlet, produced by four interacting environmental factors: storm, runoff, soil moisture and land cover. To generalise the expression and take into account the role of weathering in erosion, an erosive action of rainfall is accounted for, which is derived not only from the amount of rainfall, but also from its seasonal maximum intensity. In this way, simplifying, we have developed a model concept, translated into the semi-empirical Environmental Upscaling Sediment Erosion Model $(EUSEM)_{ORB}$, on an annual basis (Mg km^{-2} yr^{-1}), by arranging and developing the algorithm of Foster et al. [48] and Thornes [49]:

$$\mathrm{EUSEM}_{(\mathrm{ORB})} = A \cdot [(R_S + R_Q + ELT) \cdot e^{-0.07 \cdot VCP}] \quad (1)$$

where: A is a scale parameter to convert the term in brackets to Mg km^{-2} yr^{-1}, which is defined from the geographical features of the basin; R_S, R_Q, ELT and VCP define the physical structure of the system under study. R_S and R_Q are two indicators of soil erosion introduced by Foster et al. [48] to improve the erosivity factor (R_S) and take into account the effect of runoff shear stresses on soil detachment (R_Q). In particular, R_S is the rainfall erosivity indicator (unitless)

most associated with splash erosion. In this regard, Sweeney et al. [60] showed that rainsplash-driven disturbance is a robust proxy for hillslope transport, such that increasing hillslope transport efficiency decreases drainage density. R_Q is the erosivity indicator (unitless) most closely associated with surface flow. *ELT* is the erosional landscape transport component of the model, which was designed to capture the long-term memory interaction between precipitation and the basin, given the width of the ORB. Fig 4 depicts the role of mesoscale showers in erosional transport at the basin scale, assuming that the distribution of local showers is important in determining sediment-rich torrential flows in individual catchments in the basin. The term $e^{(-0.07 \cdot VCP)}$ is the exponential vegetation cover function of Thornes [49], which contains the erosivity resistance of raindrops to interril sediment detachment and transport (where *VCP* is the percentage of vegetation cover).

The R_s term introduces a threshold-type non-linearity, which is physically meaningful and necessary to obtain reasonable estimates [61], since raindrop splash plays an important role in flow-driven detachment and solute transport [62, 63]. The rain-splash component was arranged in the following form:

$$R_S = dx^{(\sigma \cdot f(rh_{mx}) + BF(S_{m-mx}))} \tag{2}$$

where dx is the maximum daily rainfall in mm in each year at Grosseto station, $f(rh_{mx})$ and $BF(S_{m\text{-}mx})$ are factors which, when combined, define the order of magnitude of the processes. In particular, $f(rh_{mx})$ is a scale factor that modulates the maximum annual hourly rainfall intensity, described as:

$$f(rh_{mx}) = \left(1 - \Omega \cdot cos\left(6.28\frac{j+\eta}{\varphi - j}\right)\right) \tag{3}$$

$BF(S_{m\text{-}mx})$ is a binary factor related to the maximum monthly soil moisture: it equal to 1, when in that year dx (at Grosseto station) > 40 mm and $S_{m\text{-}mx} > 1$ simultaneously, and equal to 0 in all other cases; j represents the month in which the maximum daily rainfall (dx) falls. This is in line with a multi-factor analysis, which showed that including the effect of rainfall intensity increases sediment yield by about 24% compared to the single most important factor, i.e., rainfall duration [64].

The terms σ, Ω, η, ϑ and φ are calibrated parameters; $S_{m\text{-}mx}$ is a function similar to $f(rh_{mx})$ but with opposite trend, to modulate the annual maximum soil moisture:

$$S_{m-mx} = \left(1 + \Omega \cdot cos\left(6.28\frac{j+\vartheta}{\varphi - j}\right)\right) \tag{4}$$

Eq (4) produces interannual variations in maximum soil moisture, based on the fact that changes in surface conditions are important contributors to runoff and sediment erosion processes [65]. This is also of great importance to further summarise the relationships between peak runoff propagation and sediment yield [63], and to understand the change in sediment erosion associated with different rainfall events [66]. The erosivity indicator R_Q, which is more associated with runoff erosion, was developed as follows:

$$R_Q = P_a(\mathrm{GRO}) + P_a(\mathrm{MON}) - B \tag{5}$$

where P_a is the annual rainfall amount (mm) at Grosseto (GRO) and Montalcino (MON) stations, respectively.

As basin morphology controls the localised forces acting to transport sediment from the eroding landscape downstream, the spatial variability of valley confinement may be important in the connectivity of hillslopes to river channels and sediment delivery to valley corridors

[67]. We thus use the *ELT* indicator as the sediment transport of landscape erosion to accomodate this process:

$$ELT = \psi \cdot P_{a-1}(\mathrm{MON}) \tag{6}$$

which assumes the importance of local storm events, which are grouped by their scale according to the communication delays between each component of the spatio-temporal hydrological integration of the basin [14]. In fact, the events affected by the precipitaion are those of the antecedent year ($P_{a\text{-}1}$) as opposed to those of the sediment estimate. This makes it explicit that floodplain sediments retained in the previous year are removed in the following year. Actually, upland areas are generally considered erosive landscapes, but at the same time they can retain sediment along river corridors and floodplains [68].

2.5. Model parameterisation and evaluation

The parameters that are required to carry out the applications of our model are defined by the model structure that best represents the processes at work, in a way that model conforms to the 'real world data', and that it discerns the processes and their interactions [53]. The constrained model parameters were derived from physical considerations, translated into empirical correlations base on observed data. The *upscaling* issue formulated here was optimised using both the runoff indicator, Eq (5), and the exponential vegetation function of Thornes [49], which has also been integrated to ensure that the formulation of a process at a point-location is somehow approximated over an area as large as a homogeneous basin unit. Througout the calibration process, special attention was paid to the use of sensitive parameters, which were carefully calibrated against high quality datasets to ensure that the resulting model would produce reliable estimates even over historical periods. The optimisation of the model was carried out through a trial-and-error procedure in which the model parameters were modified and a goodness-of-fit measure between the model results and the calibration dataset was checked [53]. This process was repeated iteratively to obtain the best possible fit between observed and predicted data, until the following criteria were met:

$$\begin{cases} R^2 = max \\ MAE = min \\ \lim_{n\to\infty}(a = 0 \& b = 1) \end{cases} \tag{7}$$

The goodness-of-fit $0 \leq R^2 \leq 1$ (optimum) was maximised to quantify the strength of a linear relationship between observations and estimates, while the second condition minimises the mean absolute error (optimum) $0 \leq MAE < \infty$. Due to the limited calibration sample and the lack of a direct validation dataset, the third condition applied is to minimise the regression line distortion between observations and estimates from the 1:1 identity line (unit slope and null intercept) as the number of samples (the vector of data) increases. Spreadsheet-based modelling was developed using the free online statistical software STATGRAPHIC (http://www.statpoint.net/default.aspx), with graphical support from AnClim (http://www.climahom.eu/software-solution/anclim [69]) and CurveExpert Professional 1.6 (https://www.curveexpert.net).

In order to also estimate the gross soil erosion (*SGE*) for comparison with the tolerable soil loss, the *SGE* in the basin was predicted as:

$$SGE = \frac{EUSEM_{ORB}}{SDR} \tag{8}$$

with *SDR* the sediment delivery ratio, calculated according to Diodato and Grauso [70]:

$$SDR = 0.416 \cdot \left(\frac{S^{0.5} \cdot \sqrt{A} \cdot (500 - \sqrt{E})}{\bar{P}_a} \right)^{-0.422} \quad (9)$$

where S is the mean slope (0.16), A is the area (2657 km^2), and E is the mean elevation (346 m a.s.l.) of the basin, and P_a is the mean annual recipitation (924 mm) over the basin [71].

3. Results and discussion

3.1. Model parameterisation and evaluation

The criteria of Eq (7) were matched with the following calibrated parameter values: A = 35.91 in Eq (1), σ = 0.70 in Eq (2), Ω = 0.50, η = 4.0 and φ = 26 in Eq (3) and Eq (4), ϑ = 1.0 in Eq (4), B = 1000 in Eq (5) and ψ = 0.10 in Eq (6). A highly significant regression (p~0.00) was achieved between actual and predicted data, with the R^2-statistic indicating that the EUSEM$_{(ORB)}$ explains 90% of sediment erosion variability. The mean absolute error (*MAE*), adopted to evaluate the amount of error, was equal to 92 Mg km^{-2} yr^{-1}, which is lower than to the standard error of the residuals (121 Mg km^{-2} yr^{-1}). The third criterion of Eq (7) was verified to have a limited distortion, as the parameters α (intercept) and b (slope) of the equation EUSEM(Y) = a +b·X tended to 0 and 1, respectively, as the number of data-points increased from 10 to 28 (with an intercept deviation of 61.1 Mg km^{-2} d^{-1} and a slope ranging between 0.92 and 1.04).

Fig 6A refers to the calibration outputs of the regression model (black line) for 28 erosion loss data-points (i.e. one determination per year). The data-points are aligned along the 1:1 red line observed data, and there is a statistically significant relationship between observed (y) and predicted (x) data: y = 0.40(±41)+1.00(±0.06); p<0.05. Only one data-point from the year 1965 (not shown in Fig 5A), was outside the confidence limit because the Grosseto station in that year had under-represented the rainfall over the basin. This is due to the disproportionate

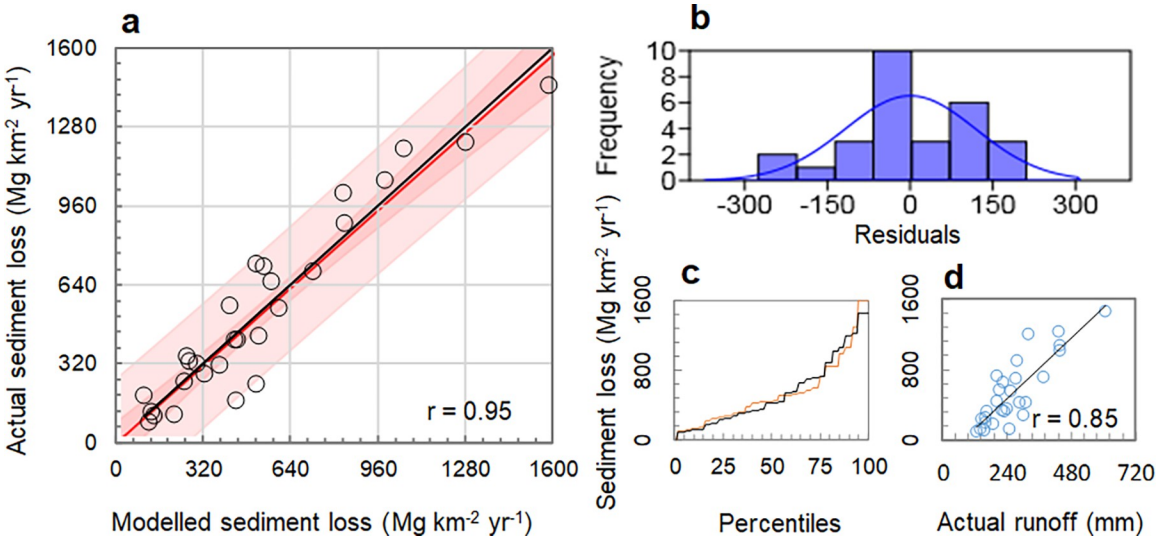

Fig 6. Model evaluation. a) Scatterplot (black regressIon line and red identity line) of experimental versus modelled–Eq (1)–sediment loss (Mg km^{-2} yr^{-1}) at the outlet of the Ombrone River Basin in the years 1949–1977 (excluding the outlier year 1965), with inner and outer boundaries showing the prediction limits for the new observations at a confidence level of 0.90 (bright pink coloured area) and 0.95 (light pink coloured area), b) histogram of residuals between actual and modelled sediment loss with Gaussiam shape (blue curve), c) percentile distribution of actual (black line) and modelled (orange line) sediment loss, d) scatterplot between the annual observed runoff and one sediment loss values (Mg km^{-2} yr^{-1}), with regression line (black line).

https://doi.org/10.1371/journal.pwat.0000072.g006

Table 1. Summary statistics of the predicted and observed sediment loss.

Sediment loss	Predicted	Observed
Count	28	28
Mean (Mg km^{-2} yr^{-1})	530	530
Standard deviation (Mg km^{-2} yr^{-1})	361	380
Coefficient of variation (%)	68	72
Minimum (Mg km^{-2} yr^{-1})	107	83
Maximum (Mg km^{-2} yr^{-1})	1588	1450
Range (Mg km^{-2} yr^{-1})	1481	1367
Standardised skewness	2.82	1.93

https://doi.org/10.1371/journal.pwat.0000072.t001

annual rainfall, with the western part of the basin receiving twice as much water as the eastern part.

Fig 6B shows a skew-free distribution of the model residuals in a Gaussian-like pattern. The percentile distribution of the modelled sediment loss (Fig 6C, orange line) approached the distributional shape of the observed discharge (Fig 6C, black line), indicating a satisfactory prediction over the range of sediment values (including low and high data). The Durbin-Watson statistic (DW = 1.84, p = 0.31, lag-1 residual autocorrelation of 0.07) shows that there is no indication of serial autocorrelation in the model residuals.

The summary statistics in Table 1 are similar between predicted and observed data. They confirm the satisfactory agreement between the two time-series, with only the standardised value of the skewness (2.82) marginally outside the expected range of -2 to +2 for the predicted sediment loss. Whether this statistic indicates some departure from the normality of the predicted time-series, according to the Kolmogorov-Smirnov (K-S) test the observed and predicted time-series can be assimilated to non-significantly dissimilar distributions (maximum distance DN = 0.14, two-sided large sample K-S statistic = 0.53, approximate p-value = 0.94).

3.2 Model upscaling and relevance of the inputs

Upscaling is a critical issue in environmental modelling, as the analytical formulation of a peculiar process effective at one point may not be valid when applied to an area as large as a basin [72]. The practice of uncritically applying a scale-up factor to small-scale results to predict those occurring on a larger scale is a recurring issue in upscaling in a variety of domains [73]. Here, since the scale of the sediment output is not related to the scale of the input data in the EUSEM, we evaluated the model's ability to upscale and integrate rainfall over the entire basin by comparing the EUSEM output with observed annual runoff data for the same calibration period as EUSEM. In the scatterplot of Fig 6D, it is visible that the runoff variable explains a moderately lower variability of sediment loss (R^2 = 0.72) compared to the EUSEM (R^2 = 0.90). This suggests both that the EUSEM is well able to upscale and that runoff is not the only variable involved in the process of sedimentation of material through the ORB, and that other factors, such as those described above (storm, soil moisture and land cover), contribute to this process, reflected in the interdependence and forcing of climatic components (e.g. antecedent rainfall, extreme events), and environmental components (e.g. accumulation of material and denudation). Thus, we will now try to verify whether all the factors assimilated by the model are relevant for the purpose of the study.

There is a wide variety of regression models, differing in the types of response variable that can be explored and in the strength of the assumptions made, which require the assessment of the relative importance of the various regressors for the response variable, regardless of the

type of model [74]. To identy whether the EUSEM can be simplified, we fitted a multiple linear regression model in which no indication of serial autocorrelation is found in the residuals at the 95% confidence level. This regression describe the relationship between sediment erosion and the four independent variables *Rs*, R_Q, *ELT* and $e^{(-0.07 \cdot VCP)}$ from Eq (1). The highest p-value on the independent variables, 0.00991678, belonging to *ELT*, indicates that also this term is statistically significant. Thus, Eq (1) cannot be simplified, making it a stable, easy to interpret and usable model [75].

3.3 Annual sediment erosion historical prediction and discussions

Although there are benefits to be gained from developing models, their real value becomes apparent when they are used extensively for system prediction, when they realise the effects of environmental processes and their evolution over time [53]. Before commenting on sediment rates, it is essential to outline the historical development of the landscape that has led the ORB to its present situation in order to determine the agricultural and geomorphological context from which the basin derives (Mazzini, 1882, p. 45 [76], our translation):

> From the indications of historians and chroniclers it is possible to deduce that at the end of the fourteenth century, woods occupied an area of over 800,000 hectares in Tuscany, 35% of the total area. In the course of just over 4 and a half centuries, the extension of forests would have decreased by 44%.

This had certainly led to a hydro-geomorphological destabilisation of the basin, which at the end of the Little Ice Age made it one of the most erosive landscapes, as can be seen from the words of Zanotti (1823, p. 288 [77], our translation):

> There is perhaps no river more turbid than this [Ombrone] as from experience I have tried comparing it to the Arno and the Serchio.

This brings us to the years when our model can work and gives us a more objective and clearer evolution of sediment yield in recent times. This allows us to see the temporal evolution of the annual sediment export from ORB over the period 1942–2020 (Fig 7, black line). Based on this trend graphs, and accounting for the temporal variation in climate, weather and vegetation, the time graph is used to visualise how the combination of these factors contribute to the sediment loss from ORB. This synthetic information flow provides us with an erosive trend composed of three time-segment, in accordance with the double-shift Standard Normal Homogeneity Test (SNHT [78]), which provides two change-points in 1967 and 1986. The Pettitt test [79], which is sensitive to detecting a change-point in the middle of the time-series, detected it in 1973, confirming that a break in the transition between the 1960s and 1970s occurred. Since the distribution frequency of sediment loss was abnormally far from normal, it was preferable to transform the time-series with a Box-Cox algorithm, before estimating the change-points, as suggested by Maftei and Barbulescu [80]. Through these statistics, we can recognise the following picture (Fig 7, black line): an early and initial period 1942–1967 with a mean value of 625 Mg km^{-2} yr^{-1} (±337 Mg km^{-2} yr^{-1} standard deviation), i.e. a sediment erosion rate fat above the tolerable sediment loss (150 Mg km^{-2} yr^{-1}, corresponding to a gross erosion of 10 Mg hm^{-2} yr^{-1} [81]), and in which the climatic forcing is high and the vegetation cover low (Fig 7, green scale band below the x-axis). An intermediate interval 1968–1986, upon the which the erosion is in a declining phase, that results by competing force between climatic-descending power and continuing enhancement of vegetation, with a mean value of 233 Mg km^{-2} y^{-1} (±101 standard deviation).

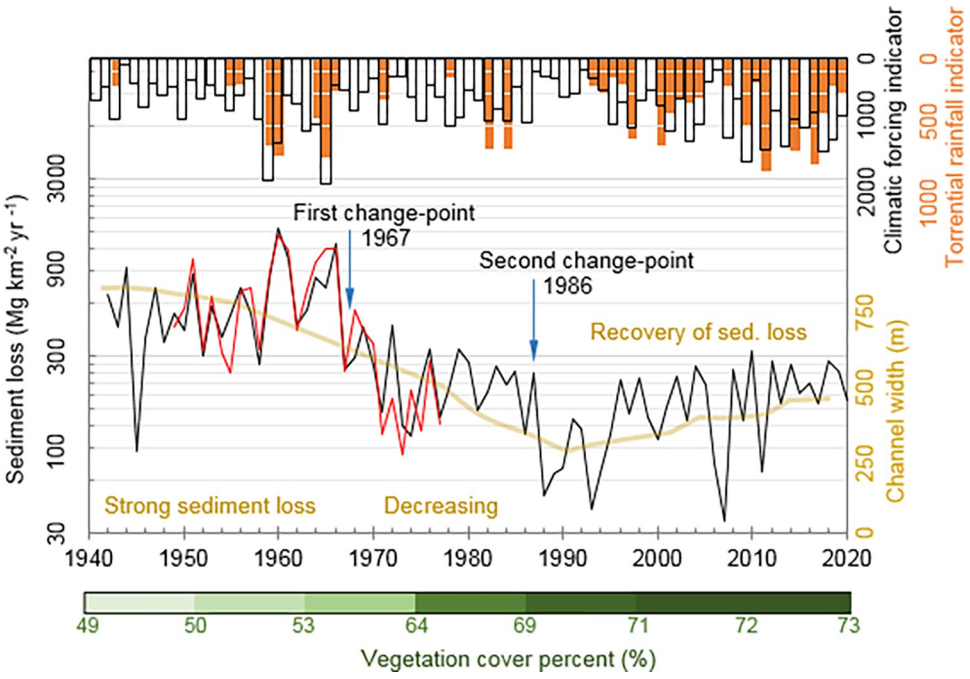

Fig 7. Temporal evolution of the estimated, Eq (1), annual amount of sediment erosion (black line), with overlapping observed data (red line) and channel width of the Trebbia River (light brown line, arranged from Bollati et al. 2014 [82]), a tributary of the Po River, with also the change-points in 1967 and 1986 derived from the Standard Normal Homogeneity Test [78]; the climatic forcing (white bars with black margins), from the climate factors in Eq (1), and the relative share of torrential rainfall (orange bars) in the Ombrone River Basin over the period 1942–2020; and the percent of vegetation cover (green scale band, from Goldewijk et al. [58]). The left-hand y-axis is in logarithmic scale.

https://doi.org/10.1371/journal.pwat.0000072.g007

The third and final period is 1987–2020, during which sediment rates are recovering. Thus, we can observe how the actual evolution of net erosion, which after a decade of low erosion rate, before 1996, sees an irregular growth that reaches an unsustainable erosion rate (sediment erosion >160 Mg km^{-2} yr^{-1}), after this date. This is also in agreement with the resuts of Borrelli et al. [37], who found areas in Tuscany where soil loss classes are above the tolerable rates and where a progressive decrease of the ability of soils to sustain vegetation and livestock dominates. The evolution of soil erosion seems still to be in line with the results of Bollati et al. [82], where the Trebbia River channel width (Fig 7, light brown line, Emilian Apennines) and phasing trends are in tandem with the progress of ORB erosion and roughly correspond to the change-points recalled above (Fig 7). The overlapping of this trend reveals three temporal phases. The first, short phase 1941–1955, refers to a first period of narrowing caused mainly by basin-wide land-use changes, a partial reduction of lateral mobility due to bank protection and artificial embankments, and a decrease of sediment delivery caused by the end of manual farming. The second, longer phase 1956–1990 of narrowing and incision began in the 1950s and was mainly related to intensive sediment collection and the introduction of agricultural mechanisation. The third and last phase 1991–2020, focuses on the most recent time of reversal of the channel width along with a partial recovery of the channel morphology. If we now estimate the coefficient of variation of sediment loss between the two change-points, and between the last change-point and the end of the time-series, it jumps from 0.43 in the period 1968–1986 to 0.50 over 1987–2020.

Even if the year 1990 was taken as a change of phase, instead of 1986 (detected change-point), the evolution associated with the coefficient of variation would not change. This has

aggravated the hazard associated with erosive phenomena, which are mainly due to episodes of torrential rains, which, although interspersed with more or less long phases of inter-storms, have increased in this period (Fig 7, orange histogram). This is in agreement with the data of Montini and Mazzanti [83], who see after 1985 an increase in annual maximum daily rainfall over the Northern Apennine district, which also includes the Ombrone basin. Of particular interest is the fact that this trend advances in tandem with global and continental (European) extreme daily precipitation, in both observations and climate models [84].

With particular reference to the ORB, the trend of sediment erosion could also be due to the abandonment and regrowth of cropland [85]. It should also be emphasised that, while the long-term trend is forced by vegetation cover, and secondarily by climate, the peaks in sediment loss are determined by storms during particularly wet periods. Accordingly, Della Seta et al. [86] observed that water erosion has a strong effect on catchment areas sediments through severe denudation events triggered by many days of rainfall, with a pulsating trend in the hillslope process that reflects the step-like pattern of denudation graphs [17], with critical denudation phases possibly triggered by extreme rainfall events [69]. However, variations in sediment erosion may also contribute to a complex interplay between land-use changes that have affected the study-area, revealing a delicate balance between farming activities and erosion processes [87, 88].

4. Conclusion

The reconstruction of the temporal evolution of sediment loss (1942–2020) in a key landscape basin unit of central Italy (the Ombrone River Basin) can be useful to assess the current evolution of erosional processes in Mediterranean environments. The modelling approach adopted allowed a quantitative assessment of eroded sediment loss, where a combination of climatic and vegetation data provided a sufficiently detailed morpho-evolutionary picture of the basin area studied. The model developed here thus has a role to play in estimating net erosion thanks to its potential to capture temporal dynamics over long time-series in the absence of detailed input data (parsimonious approach). The satisfactory evaluation of the model (with respect to the data sampled in 1949–1977 and, indirectly, against the width of another river in western Italy, the Trebbia River) is a clue that the drivers and the parameterisation used reflect the interannual distribution of sediment loss over the whole basin. These features increase the scientific value of this study, especially with regard to modelling, didactic simplicity and the environmental supporting role of the investigated landforms.

Supporting information

S1 Text. Data used for model calibration (1949–1977).
(TXT)

S2 Text. Data used for reconstruction (1942–2020).
(TXT)

S3 Text. Extracts from historical sources.
(TXT)

Author Contributions

Conceptualization: Nazzareno Diodato.

Data curation: Nazzareno Diodato.

Formal analysis: Nazzareno Diodato.

Funding acquisition: Fredrik Charpentier Ljungqvist.

Investigation: Nazzareno Diodato.

Methodology: Nazzareno Diodato.

Project administration: Nazzareno Diodato.

Resources: Nazzareno Diodato.

Software: Nazzareno Diodato.

Supervision: Gianni Bellocchi.

Validation: Nazzareno Diodato, Francesco Fiorillo.

Visualization: Nazzareno Diodato.

Writing – original draft: Nazzareno Diodato.

Writing – review & editing: Nazzareno Diodato, Fredrik Charpentier Ljungqvist, Francesco Fiorillo, Gianni Bellocchi.

References

1. Noe GB, Cashman MJ, Skalak K, Gellis A, Hopkins KG, Moyer D, et al. Sediment dynamics and implications for management: State of the science from long-term research in the Chesapeake Bay watershed, USA. WIREs Water 2020; 7: e1454. https://doi.org/10.1002/wat2.1454
2. Kemp DB, Sadler PM, Vanacker V. The human impact on North American erosion, sediment transfer, and storage in a geologic context. Nat. Commun. 2020; 11: 6012. https://doi.org/10.1038/s41467-020-19744-3 PMID: 33243971
3. Amundson R, Berhe AA, Hopmans JW, Olson C, Sztein AE, Sparks DL. 2015. Soil and human security in the 21st century. Science 2015; 348: 1261071. https://doi.org/10.1126/science.1261071 PMID: 25954014
4. Wu L, Jiang J, Li G-X, Ma X-Y. Characteristics of pulsed runoff-erosion events under typical rainstorms in a small watershed on the Loess Plateau of China. Sci. Rep. 2018; 8: 3672. https://doi.org/10.1038/s41598-018-22045-x PMID: 29487320
5. Meng X, Zhu Y, Yin M, Dengfeng L. The impact of land use and rainfall patterns on the soil loss of the hillslope. Sci. Rep. 2021; 11: 16341. https://doi.org/10.1038/s41598-021-95819-5 PMID: 34381135
6. Van Pelt RS. Erosion by wind: environmental effects In: Lal R, editor. Encyclopedia of soil science. London: Taylor and Francis; 2011. pp. 1–7.
7. Lal B. Soil erosion by wind and water: problems and prospects. In: Lal R, editor. Soil erosion research methods. New York: Routledge; 1994. pp. 1–10. https://doi.org/10.1201/9780203739358
8. Frank S, Fürst C, Witt A, Koschke L, Makeschin F. Making use of the ecosystem services concept in regional planning–trade-offs from reducing water erosion. Landscape Ecol. 2014; 29: 1377–1391.
9. Diodato N, Ljungqvist FC, Bellocchi G. Fingerprint of climate change in precipitation aggressiveness across the central Mediterranean (Italian) area. Sci. Rep. 2020; 10: 22062. https://doi.org/10.1038/s41598-020-78857-3 PMID: 33328541
10. Sofia G, Roder G, Dalla Fontana G, Tarolli P. Flood dynamics in urbanized landscapes: 100 years of climate and humans' interaction. Sci. Rep. 2017; 7: 40527. https://doi.org/10.1038/srep40527 PMID: 28079147
11. Yin J, Gentine P, Zhou S, Sullivan SC, Wang R, Zhang Y, et al. Large increase in global storm runoff extremes driven by climate and anthropogenic changes. Nat. Commun. 2018; 9: 4389. https://doi.org/10.1038/s41467-018-06765-2 PMID: 30348951
12. Diodato N, Bellocchi G. Storminess and environmental change: Climate forcing and response in the Mediterranean region. Dordrecht: The Netherlands; 2014. https://doi.org/10.1007/978-94-007-7948-8
13. Corella J, Valero-Garcés B, Vicente-Serrano SM, Brauer A, Benito G. Three millennia of heavy rainfalls in Western Mediterranean: frequency, seasonality and atmospheric drivers. Sci. Rep. 2016; 6: 38206. https://doi.org/10.1038/srep38206 PMID: 27910953

14. Diodato N, Borrelli B, Panagos P, Bellocchi G, Bertolin C. Communicating hydrological hazard-prone areas in Italy with geospatial probability maps. Front. Environ. Sci. 2019; 7: 193. https://doi.org/10.3389/fenvs.2019.00193

15. Sereni E. Storia del paesaggio agrario italiano. Bari: Laterza; 1961. Available from: https://www.google.fr/books/edition/Storia_del_paesaggio_agrario_italiano/SBjbAAAAMAAJ?hl=en&gbpv=1&bsq=%22Storia+del+paesaggio+agrario+Italiano%22&dq=%22Storia+del+paesaggio+agrario+Italiano%22&printsec=frontcover. (in Italian).

16. Alberti L. Descrittione di tutta Italia. Venice: Altobello Salicato; 1588. Available from: https://books.google.fr/books?id=KdclEEV28MsC&printsec=frontcover&hl=it&source=gbs_ge_summary_r&cad=0#v=onepage&q&f=false (in Italian).

17. Della Seta M, Del Monte M, Fredi P, Lupia Palmieri E. Direct and indirect evaluation of denudation rates in Central Italy. Catena 2007; 71: 21–30.

18. Ciccacci S, Galiano MC, Roma MA, Salvatore MC. Morphological analysis and erosion rate evaluation in badlands of Radicofani area (Southern Tuscany–Italy). Catena 2008; 74: 87–97.

19. Vallebona C, Mantino A, Bonari E, 2016. Exploring the potential of perennial crops in reducing soil erosion: A GIS-based scenario analysis in southern Tuscany, Italy. Appl. Geogr. 66: 119–131.

20. Fang N-F, Shi Z-H, Yue B-J, Wang L. The characteristics of extreme erosion events in a small mountainous watershed. PLOS One 2013; 8: e76610. https://doi.org/10.1371/journal.pone.0076610 PMID: 24146898

21. Napoli M, Dalla Marta A, Zanchi CA, Orlandini S. Assessment of soil and nutrient losses by runoff under different soil management practices in an Italian hilly vineyard. Soil Tillage Res. 2017; 168: 71–80.

22. Tarragoni C, Bellotti P, Davoli L. Natural and anthropogenic forcing during the last two centuries in the Ombrone delta (Central Italy). Ital. J. Eng. Geol. Environ. 2015; 1, 5–16.

23. Borrelli P, Robinson DA, Fleischer LR, Lugato E, Ballabio C, Alewell C, et al. An assessment of the global impact of 21st century land use change on soil erosion. Nat. Commun. 2017; 8: 2013. https://doi.org/10.1038/s41467-017-02142-7 PMID: 29222506

24. Zhang J, Shang Y, Liu J, Fu J, Wei S, Tong L. Causes of variations in sediment yield in the Jinghe River Basin, China. Sci. Rep. 2020; 10: 18054. https://doi.org/10.1038/s41598-020-74980-3 PMID: 33093547

25. Hateffard F, Mohammed S, Alsafadi K, Enaruvbe GO, Heidari A, Abdo HG, et al. CMIP5 climate projections and RUSLE-based soil erosion assessment in the central part of Iran. Sci. Rep. 2021; 11: 7273. https://doi.org/10.1038/s41598-021-86618-z PMID: 33790351

26. Cevasco A, Diodato N, Revellino P, Fiorillo F, Grelle G, Guadagno FM. Storminess and geo-hydrological events affecting small coastal basins in a teraced Mediterranean environment. Sci. Total Environ. 2015; 532: 208–219.

27. Märker M, Angeli L, Bottai L, Costantini R, Ferrari R, Innocenti L, et al. Assessment of land degradation susceptibility by scenario analysis: A case study in Southern Tuscany, Italy. Geomorphology 2008; 93: 120–129.

28. DAS. Unit of Management: Ombrone (ITADBR093). Regione Toscana, Piano di gestione rischio alluvioni. Florence, Distretto Appennino Settentrionale; 2016. Available from: http://www.appenninosettentrionale.it/rep/UOM/UoM_Omb_pa_01.pdf. (in Italian).

29. Trigila A, Iadanza C, Berti D, Lucarini M. Principali eventi franosi e alluvionali in Italia tra il 2003 e il 2014. Rome: Istituto Superiore per la Protezione e la Ricerca Ambientale; 2015. Available from: https://www.isprambiente.gov.it/files/temi/Rapporto_Eventi_frane_alluvioni_ISPRA_Febbraio_2015.pdf. (in Italian).

30. CFRT. Servizio Idrologico. Report eventi meteo-idrologici dei giorni 10, 11 e 12 November 2012. Florence: Centro Funzionale della Regione Toscana; 2012. Available from: https://www.cfr.toscana.it/index.php?IDS=23&IDSS=191. (in Italian).

31. Zanchini E, Nanni G, Minutolo A. Rapporto 2020: Il clima è già cambiato. Rome: Legambiente, UNIPOL–ENEL; 2020. Available from: https://cittaclima.it/2020/11/10/presentazione-del-rapporto-2020-dellosservatorio-di-legambiente-cittaclima. (in Italian).

32. ARAAT. Annali della Regia Accademia di Agricoltura di Torino. Turin: Chirio e Mina; 1904. Available from: https://www.google.it/books/edition/Annali/jMUiAQAAIAAJ?hl=it&gbpv=1&bsq=annali+Il+disboscamento+che+si+va+spesso+compiendo+inconsultamente+nell%E2%80%99Appennino&dq=annali+Il+disboscamento+che+si+va+spesso+compiendo+inconsultamente+nell%E2%80%99Appennino&printsec=frontcover. (in Italian).

33. Sepuru TK, Dube T. An appraisal on the progress of remote sensing applications in soil erosion mapping and monitoring. Remote Sens. Appl.: Soc. Environ. 2018; 9: 1–9. https://doi.org/10.1016/j.rsase.2017.10.005

34. Foreman MGG, Stucchi DJ, Garver DJ, Tuele KA, Isaac D, Grime J, et al. A circulation model for the Discovery Islands, British Columbia. Atmos. Ocean. 2012; 50: 301–316. https://doi.org/10.1080/07055900.2012.686900

35. Tejedor E, Saz MA, Cuadrat JM, Esper J, de Luis M. Temperature variability in the Iberian range since 1602 inferred from tree-ring records. Clim. Past 2017; 13: 93–105. https://doi.org/10.5194/cp-13-93-2017

36. Walling DE, Fang D. Recent trends in the suspended sediment loads of the world's rivers. Global Planet. Change 2003; 39: 111–126. https://doi.org//10.1016/S0921-8181(03)00020-1

37. Borrelli P, Paustian K, Panagos P, Jones A, Schütt B, Lugato E. Effect of good agricultural and environmental conditions on erosion and soil organic carbon balance: a national case study. Land Use Policy 2016; 50: 408–421. https://doi.org/10.1016/j.landusepol.2015.09.033

38. de Vente J, Poesen J. Predicting soil erosion and sediment yield at the basin scale: scale issues and semi-quantitative models. Earth-Sci. Rev. 2005. 71: 95–125. https://doi.org/10.1016/j.earscirev.2005.02.002

39. Chiverrell RC, Foster GC, Thomas GSP, Marshall P. Robust chronologies for landform development. Earth Surf. Process. Landf. 2009; 34: 319–328. https://doi.org/10.1002/esp.1720

40. Wischmeier WH, Smith DD. Predicting rainfall erosion losses from cropland east of the Rocky Mountains: Guide for selection of practices for soil and water conservation, Issues 282–290. Brooksville FL: Agricultural Handbook 282; U.S. Department of Agriculture; 1965.

41. Foster GR, Toy TE, Renard KG. Comparison of the USLE, RUSLE1.06 and RUSLE2 for application to highly disturbed lands. In: Renard KG, Mc. Ilroy SA, Gburek WJ, Cranfield HE, Scott RL, editors, Proceedings of the First interagency conference on research in watersheds; October 27–30, 2003. Benson AZ: U.S. Department of Agriculture; 27, pp. 154–160.

42. Borrelli P, Van Oost K, Meusburger K, Alewell C, Lugato E, Panagos P. A step towards a holistic assessment of soil degradation in Europe: Coupling on-site erosion with sediment transfer and carbon fluxes. Environmental Research 2018; 161: 291–298. https://doi.org/10.1016/j.envres.2017.11.009 PMID: 29175727

43. Kinnel PIA. Event soil loss, runoff and the Universal Soil Loss Equation family of models: A review. J. Hydrol. 2010; 385: 384–397. https://doi.org/10.1016/j.jhydrol.2010.01.024

44. Gericke A, Venohr M. Improving the estimation of erosion-related suspended solid yields in mountainous, non-alpine river catchments. Environ. Model. Softw. 2012; 37: 30–40. https://doi.org/10.1016/j.envsoft.2012.04.008

45. Diodato N, Gericke A, Bellocchi G. Modelling the inter-annual variability of sediment yields: A case study for the upper Lech River. Catena 2012; 97: 12–19. https://doi.org/10.1016/j.catena.2012.04.013

46. Diodato N, de Vente J, Bellocchi G, Guerriero L, Soriano M, Fiorillo F, et al. Estimating long-term sediment export using a seasonal rainfall-dependent hydrological model in the Glonn River basin, Germany. Geomorphology 2015; 228: 628–636. https://doi.org/10.1016/j.geomorph.2014.10.011

47. Diodato N, Mao L, Borrelli P, Panagos P, Fiorillo F, Bellocchi G. Climate-scale modelling of suspended sediment load in an Alpine catchment debris flow (Rio Cordon-northeastern Italy). Geomorphology 2018; 309: 20–28. https://doi.org/10.1016/j.geomorph.2018.02.026

48. Foster GR, Meyer LD, Onstad CA. A runoff erosivity factor and variable slope length exponents for soil loss estimates. Trans. ASAE 1977; 20: 683–687.

49. Thornes JB. The interaction of erosional and vegetational dynamics in land degradation: Spatial outcomes. In: Thornes JB, editor. Vegetation and erosion. Chichester: Jonh Wiley & Sons; 1990. pp. 45–55.

50. Diodato N, Bellocchi G. Reconstruction of seasonal net erosion in a Mediterranean landscape (Alento River Basin, Southern Italy) over the past five decades. Water 2019; 11: 2306. https://doi.org/10.3390/w11112306

51. Diodato N, Fiorillo F, Rinaldi M, Bellocchi G. 2022. Environmental drivers of dynamic soil erosion change in a Mediterranean fluvial landscape. PLoS One 2022; https://doi.org/10.1371/journal.pone.0262132 PMID: 35061741

52. Francis CF, Thornes JB. Runoff hydrographs from three Mediterranean vegetation cover types. In: Thornes JB, editor. Vegetation and erosion, processes and environments. Chichester: Wiley; 1990, pp. 363–384.

53. Mulligan M, Wainwright J. Modelling and model building. In: Wainwright J, Mulligan M, editors. Environmental modelling: finding simplicity in complexity. Chichester: Wiley; 2004. pp. 7–73.

54. SIMN. Hydrological annals. Rome: Servizio Idrografico and Mareografico Nazionale Italiano; 1949–1977. Available from: https://www.isprambiente.gov.it/it/progetti/cartella-progetti-in-corso/acque-interne-e-marino-costiere-1/progetti-conclusi/progetto-annali/gli-annali-idrologici. (in Italian).

55. Oosterbroek P. Biodiversity of the Mediterranean region. In: Forey PL, Humphries CJ, Vane-Wright R. I., editors. Systematics and conservation evaluation. The Systematics Association Special Volume No. 50. Oxford: Clarendon Press; 1994. pp. 289–307.

56. Toscana Regione. Piano paesaggistico: Maremma grossetana. Florence: Regione Toscana; 2014a. Available from: https://www.regione.toscana.it/-/piano-di-indirizzo-territoriale-con-valenza-di-piano-paesaggistico. (in Italian).

57. Iannuccilli M. Classificazione dei tipi di tempo e alluvioni in Toscana, nel contesto dei cambiamenti climatici. Florence; LAMMA, Tipografia del Consiglio Regionale della Toscana; 2016. Available from: https://www.slideshare.net/alfcrisci/classificazione-tipi-di-tempo-e-alluvioni-in-toscna. (in Italian).

58. Goldewijk KK, Beusen A, Doelman J, Stehfest E. Anthropogenic land use estimates for the Holocene–HYDE 3.2. Earth Syst. Sci. Data 2017; 9: 927–953. https://doi.org/10.5194/essd-9-927-2017

59. Toy TJ, Foster GR, Renard KG. Soil erosion; prediction, measurement, and control. New York, NY: John Wiley & Sons; 2002.

60. Sweeney KE, Roering JJ, Ellis CS. Experimental evidence for hillslope control of landscape scale. Science 2015; 349, 51–53.

61. Ye W, Bates BC, Viney NR, Sivapalan M, Jakeman AJ Performance of conceptual rainfall-runoff models in low-yielding ephemeral catchments. Water Resour. Res. 1997; 33: 153–166.

62. Tao W, Wu J, Wang Q. Mathematical model of sediment and solute transport along slope land in different rainfall pattern conditions. Sci. Rep. 2017; 7: 44082. https://doi.org/10.1038/srep44082 PMID: 28272431

63. Zi T, Kumar M, Albertson J. Intercomparing varied erosion, deposition and transport process representations for simulating sediment yield. Sci. Rep. 2019; 9: 12029. https://doi.org/10.1038/s41598-019-48405-9 PMID: 31427646

64. Shojaei S, Kalantari Z, Rodrigo-Comino J. Prediction of factors affecting activation of soil erosion by mathematical modeling at pedon scale under laboratory conditions. Sci. Rep. 2020; 10: 20163. https://doi.org/10.1038/s41598-020-76926-1 PMID: 33214590

65. Zhang FB, Bai YJ, Xie LY, Yang MY, Li ZB, Wu XR, et al. Runoff and soil loss characteristics on loess slopes covered with aeolian sand layers of different thicknesses under simulated rainfall. J. Hydrol. 2017; 549: 244–251.

66. Wu X, Guo S, Yin J, Yang G, Zhong Y, Liu D. On the event-based extreme precipitation across China: Time distribution, trends and return levels. J. Hydrol. 2018; 562: 305–417.

67. Wohl E, Hall RO Jr, Lininger KB, Sutfin NA, Walters DM. Carbon dynamics of river corridors and the effects of human alterations. Ecol. Monogr. 2017; 87: 379–409.

68. Sutfin NA, Wohl E. Elevational differences in hydrogeomorphic disturbance regime influence sediment residence times within mountain river corridors. Nat. Commun. 2019; 10: 2221. https://doi.org/10.1038/s41467-019-09864-w PMID: 31110171

69. Štěpánek P. AnClim–software for time series analysis. Brno: Faculty of Natural Sciences, Masaryk University, 2005. Available from: http://www.climahom.eu/software-solution/anclim.

70. Diodato N, Grauso S. An improved correlation model for sediment delivery ratio assessment. Environ. Earth Sci. 2009; 59: 223–231.

71. Cavazza S. Regionalizzazione geomorfologica del trasporto solido in sospensione dei corsi d'acqua tra il Magra e l'Ombrone. Atti Soc. Tosc. Sci. Nat., Mem., Serie A 1984; 91: 119–132. (in Italian).

72. Danny Harvey LD. Climate and climate-system modelling. In: Wainwright J, Mulligan M, editors. Environmental modelling: finding simplicity in complexity. Chichester: Wiley; 2004. pp. 77–91.

73. Balgobin T, Evrard D. A framework for modelling emerging processes' upscaling from an environmental perspective. Procedia CIRP 2020; 90: 154–158.

74. Grömping U. Variable importance in regression models. WIREs Comput Stat. 2015; 7: 137–152.

75. Royston P, Sauerbrei W. Multivariate model-building. Chichester: John Wiley & Sons; 2008.

76. Mazzini CM. La Toscana agricola; sulle condizioni dell' agricoltura e degli agricoltori nelle provincie di Firenze, Arezzo, Siena, Lucca, Pisa e Livorno. Florence, Paggi; 1882. Available from: https://babel.hathitrust.org/cgi/pt?id=hvd.hndgeh&view=1up&seq=7. (in Italian).

77. Zanotti E Opere idrauliche. Raccolta d'Autori Italiani che trattano del Moto dell'Acque, To. VII. Bologna: Tipografia Marsigli; 1823. Available from: https://books.google.fr/books?id=2vYCDQntXFoC&newbks=0&printsec=frontcover&pg=PA264&dq=%221823%22+%22opere+idrauliche%22+Raccolta+d%27Autori+Italiani+che+trattano+del+Moto+delle%E2%80%99Acque%22+%22Tomo+VII%22&hl=en&source=newbks_fb&redir_esc=y#v=onepage&q&f=false. (in Italian).

78. Alexandersson H, Moberg A. Homogenization of Swedish temperature data. Part I: homogeneity test for linear trends. Int. J. Climatol. 1997; 17: 25–34.

79. Pettitt AN. A non-parametric approach to the change point problem. Appl. Stat. 1979; 28, 126–135.

80. Maftei C, Barbulescu A. Statistical analysis of precipitation time series in Dobrudja region. MAUSAM 2012; 63: 553–564.

81. Morgan RPC. Soil erosion and conservation. Hoboken, NJ: John Wiley & Sons; 2005.

82. Bollati IM, Pellegrini L, Rinaldi M, Duci G, Pelfini M Reach-scale morphological adjustments and stages of channel evolution: The case of the Trebbia River (northern Italy). Geomorphology 2014; 221: 176–186.

83. Montini G., Mazzanti B. Analisi del cambiamento climatico nel Distretto Appennino Settentrionale e individuazione delle criticità di Piano. Florence: Autorità di Bacino del Fiume Arno; 2015. Available from: https://www.regione.toscana.it/documents/10180/14410215/Le%20aree%20sciistiche%20della%20toscana.pdf/2f27ec1e-5aff-4fc9-8254-4c8f949c0714. (in Italian).

84. Donat M, Lowry A, Alexander L, O'Gorman PA, Maher N. More extreme precipitation in the world's dry and wet regions. Nature Clim. Change 2016; 6: 508–513.

85. Vergari F, Della Seta M., Del Monte M, Fredi P, Lupia Palmieri E Long- and short-term evolution of several Mediterranean denudation hot spots: The role of rainfall variations and human impact. Geomorphology 2013; 183, 14–27.

86. Della Seta M, Del Monte M, Fredi P, Lupia Palmieri E. Space-time variability of denudation rates at the catchment and hillslope scales on the Tyrrhenian side of Central Italy. Geomorphology 2009; 107: 161–177.

87. Bollati I, Della Seta M, Pelfini M, Del Monte M, Fredi P, Lupia Palmieri E Dendrochronological and geomorphological investigations to assess water erosion and mass wasting processes in the Apennines of Southern Tuscany (Italy). Catena 2012; 90: 1–17.

88. Aucelli PPC, Conforti M, Della Seta M, Del Monte M, D'uva L, Rosskopf CM, et al. Multi-temporal digital photogrammetric analysis for quantitative assessment of soil erosion rates in the Landola catchment of the Upper Orcia Valley (Tuscany, Italy). Land Degrad Dev 2016; 27: 1075–1092.

89. Toscana Regione. Piano paesaggistico: I paesaggi rurali storici della Toscana. Florence: Regione Toscana; 2014b. Available from: https://www.regione.toscana.it/-/piano-di-indirizzo-territoriale-con-valenza-di-piano-paesaggistico. (in Italian).

90. Borrelli P, Ballabio C, Yang J, Robinson D, Panagos P. GloSEM: High-resolution global estimates of present and future soil displacement in croplands by water erosion. Sci. Data 2022; 9: 406. https://doi.org/10.1038/s41597-022-01489-x PMID: 35831371

91. Panagos P, Borrelli P, Meusburger K, Yu B, Klik A, Lim KJ, et al. Global rainfall erosivity assessment based on high-temporal resolution rainfall records. Sci Rep 2017; 7: 4175. https://doi.org/10.1038/s41598-017-04282-8 PMID: 28646132

92. Angeli L, Chiesi M, Ferrari R, Magno R. Clima che cambia: gli impatti sul territorio Toscano. Florence: Consorzio LaMMA–CNR-IBIMET; 2012. Available from: https://www.researchgate.net/publication/264539882_Clima_che_cambia_-_Gli_impatti_sul_territorio_toscano (in Italian).